

REFERENCE 3

MFN 06-032

Research Report
ENE53/46/2000

**Investigation on Aerosol Deposition in
a Heat Exchanger Tube**

Jouni Hokkinen
Ari Auvinen
Tommi Renvall
Wolfgang Ludwig
Jorma Jokiniemi

Research Report
ENE53/46/2000

**Investigation on Aerosol Deposition in
a Heat Exchanger Tube**

Jouni Hokkinen
Ari Auvinen
Tommi Renvall
Wolfgang Ludwig
Jorma Jokiniemi

VTT Energy

P.O. Box 1601, FIN-02044 VTT, FINLAND

Phone +358 9 456 5442, Telefax +358 9 460493

Espoo, 08.01.2001

Research organisation and address VTT Energy, Engine Technology and Energy in Transportation P.O. Box 1601 FIN-02044 VTT, FINLAND Project manager Ari Auvinen Diary code 30-2000/ENE5	Customer Teollisuuden Voima Oy Fin-27610 Olkiluoto, Finland Contact person Eero Patrakka Order reference 803800/ETP , 6.3.2000	
Project title and reference code Kokeet aerosolien depositionsmekanismien tutkimiseksi 53ESBWR	Report identification & Pages ENE53/46/2000 34 p.	Date 08.01.2001

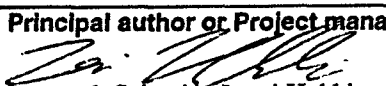
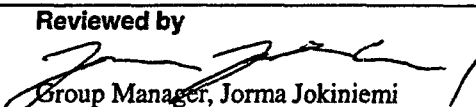
Report title and author(s)
INVESTIGATION ON AEROSOL DEPOSITION IN A HEAT EXCHANGER TUBE
Hokkinen, J., Auvinen, A., Renvall, T., Ludwig, W. and Jokiniemi, J.

Summary

Contents

Part I Facility Testing and Aerosol Measurements	
1 Introduction	3
2 Experimental set-up	4
2.1 Aerosol generation and the main flow channel	5
2.2 Aerosol sampling and dilution	6
2.3 Measuring instruments	7
2.3.1 Berner Low Pressure Impactor	7
2.3.2 TEOM 1400A	8
3 Experiments	8
3.1 Temperature and flow characteristics	8
3.2 Aerosol measurements	10
4 Results	11
4.1 Mass size distribution	11
4.2 Deposition	12
5 Discussion and conclusions	15
6 References	16
Appendices	17
Part II Radio Tracer Experiments	
1 Introduction	22
2 Requirements for the aerosol material	22
3 Experimental set-up	23
4 Calibration of the sequential detectors	24
5 Preliminary experiment	27
6 Conclusions	29
Part III Modelling	
Surface Steam Condensation in Computational Fluid Dynamics	30

Distribution

Principal author or Project manager  Research Scientist, Jouni Hokkinen	Reviewed by  Group Manager, Jorma Jokiniemi
Approved by Nils-Olof Nylund Research Manager, Engine Technology and Energy in Transportation	Availability statement

Contents

Part I Facility Testing and Aerosol Measurements

1 Introduction	3
2 Experimental set-up	4
2.1 Aerosol generation and the main flow channel	5
2.2 Aerosol sampling and dilution	6
2.3 Measuring instruments	7
2.3.1 Berner Low Pressure Impactor	7
2.3.2 TEOM 1400A	8
3 Experiments	8
3.1 Temperature and flow characteristics	8
3.2 Aerosol measurements	10
4 Results	11
4.1 Mass size distribution	11
4.2 Deposition	12
5 Discussion and conclusions	15
6 References	16
Appendices	17

Part II Radio Tracer Experiments

1 Introduction	22
2 Requirements for the aerosol material	22
3 Experimental set-up	23
4 Calibration of the sequential detectors	24
5 Preliminary experiment	27
6 Conclusions	29

Part III Modelling

Surface Steam Condensation in Computational Fluid Dynamics	30
---	-----------

1 Introduction

The aim of the work was to investigate aerosol behavior in a heat exchanger. The heat exchanger is a model of one single tube of a Passive Containment Condenser (PCC) that is used in the European Simplified Boiling Water Reactor (ESBWR). ESBWR is a new generation nuclear power plant, designed by General Electric and its European partners (Posta and Rao, 1996). In case of severe reactor accident the PCC removes excess core heat. In addition to cooling, it also has an important role mitigating offsite dose by retention of fission product release in a containment (Guntay and Suckow 1996).

Similar tests have been done with the AIDA, Aerosol Impaction and Deposition Analysis, test facility (Dehbi et al. 1997), which is a scaled down version of the actual PCC. Also Watanabe et al. (1996) have made PCC aerosol deposition experiments. The interest for the experiments in this work arose from the inconsistent results of the AIDA experiments, where three aerosol materials were used. Insoluble SnO was used together with soluble CsI. In another experiment insoluble SnO₂ was used alone. The deposition behaviour of SnO₂ in the heat exchanger was very different from the behaviour of SnO and CsI. SnO₂ deposited in such amounts that the heat removal capacity of the heat exchanger was reduced and a pressure drop was detected. SnO did not cause either of these problems (Dehbi et al. 1997).

To investigate the aerosol deposition in the heat exchanger, polydisperse aerosol was produced and the mass concentration of the aerosol was measured before and after the heat exchanger. Also the size distribution of the aerosol was characterized. The experiments were performed with hygroscopic NaCl particles in three environments: dry, low steam and high steam conditions. Furthermore, inert Cu particles were investigated in dry conditions.

The experimental set-up used in this study is an improved version of the earlier experiments (Lehtinen). In the new set-up several modifications to the earlier one were made. First, the aerosol generation has been improved so that it is more stable and able to produce high concentrations of multicomponent insoluble and soluble aerosols. Secondly, the temperature measurement of the cooling water was improved and a heater was installed to control the inlet cooling water temperature. The design of the heat exchanger was changed to achieve larger cooling water velocity with smaller flow rate. Finally, a gamma radio tracer measurement system was designed and installed to study the local

deposit behaviour in real time. First experiments were conducted with inactive aerosol to compare the system behaviour with the earlier experiments.

2 Experimental Set-up

The aim of the work was to study aerosol behaviour in a heat exchanger tube. Experiments were made with NaCl particles in three different environments: dry, low steam and high steam conditions. Furthermore, the behaviour of Cu particles was investigated. The mass concentration of the aerosol is measured before and after the heat exchanger and the size distribution of the aerosol is characterized.

2.1 Aerosol generation and the main flow channel

A schematic picture of the facility used in the experiments is presented in Fig. 1. NaCl particles were formed by vaporizing NaCl in furnace. NaCl was held in an aerodynamically shaped container that was placed in the middle of the furnace. The nitrogen flow rate through the furnace was controlled with a mass flow controller and the flow rate was set to 5.0 l/min (NTP). The dry powder generator was not used in NaCl experiments.

Copper aerosol is made with Cu powder and a TOPAS SAG 410 dry powder generator. In this case, the nitrogen flow through the dry powder generator and the furnace is 20 l/min (NTP). The dry powder generator has a built-in critical orifice that was used to control the flow.

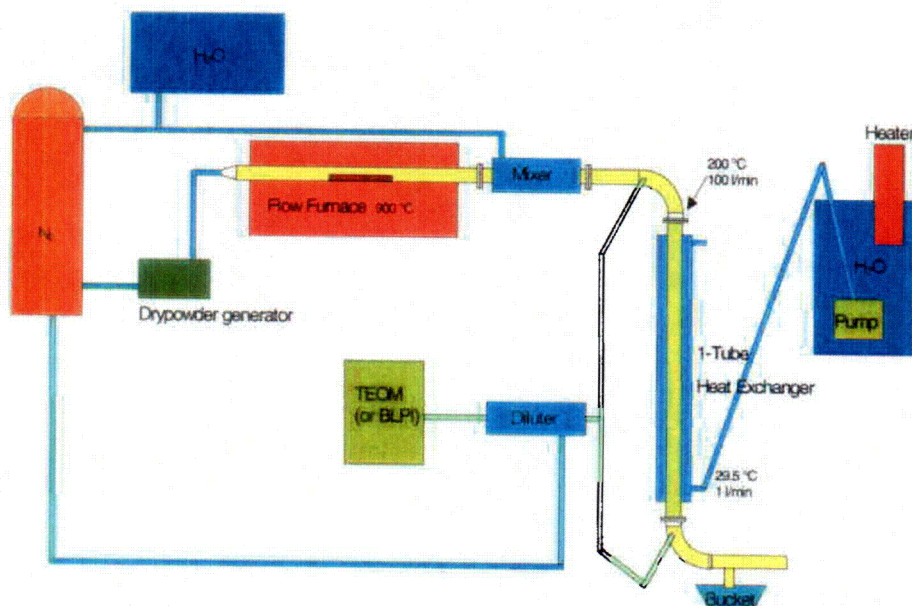


Figure 1. Experimental set-up

The nitrogen flow was directed through an ENTECH VTF 30/12 tube furnace. At the center of the furnace there was an approximately 800 mm long stainless steel tube. The inside diameter of the tube was 18.1 mm. It was heated through radiative heat transfer with KANTHAL A-1 metallic coil heating elements. The furnace was divided into two zones, both containing one element. Both zones were controlled with one Eurotherm 902/904 PID control unit. The total heated length of the furnace was 400 mm. In the experiments the temperature of the furnace was set to 900°C.

After the furnace there was a porous stainless steel mixer that combined the aerosol flow from the furnace to the main gas flow so that the total flow rate was 100 l/min (NTP). The main flow was either nitrogen or a mixture of steam and nitrogen. Both flows were controlled with proper critical orifices. Steam for the experiment was produced with a VEIT 2365 steam generator. The temperature of the main flow was close to 200°C. Between the porous stainless steel mixer and the heat exchanger there was a 50 cm long straight tube in order to allow the particles to mix uniformly in the turbulent gas flow.

The vertical heat exchanger models one tube of the PCC. The heat exchanger was built in such a way that the inner tube was removable. The total length of the removable tube was 100 cm and the length of the cooled area was 80 cm. The inner diameter of the tube was 22 mm and wall thickness 1.5 mm. The inner tube was changed after every experiment for possible later examination.

The deposition tube was cooled by water flowing upward between the deposition tube and an outer tube. The thickness of flow channel between the tubes was 5 mm. The heat exchanger had 2 inlets and 4 outlets for cooling water to achieve more uniform flow. The flow rate of the cooling water was 1.0 l/min and it was preheated to 30°C in a 60 liter tub with HAAKE DL30 circulator heater. Cooling water flow was controlled with an Aquarius 600 submersible pump. Inlet water temperature was measured also from one inlet right before the heat exchanger with Pt100 resistance type detector (RTD). The temperature gradient of the cooling water was measured with three Pt100 RTDs attached on the outer wall of the deposition tube. Temperature of outlet water was measured from one outlet with Pt100 RTD and from opposite outlet with T-type thermocouple. The four outlets were mixed and the temperature was measured with an another T-type thermocouple after mixing.

Below the heat exchanger there was a bucket, where the condensed water was collected. In NaCl impactor measurements a filter was used to collect particles. As the filter caused the system to pressurize, it could not be used in TEOM measurements. The gas flow was directed to a fume hood with a wide hose.

2.2 Aerosol sampling and dilution

In order to determine the deposition of the particles, the flow was sampled from the beginning and from the end of the heat exchanger, as shown in Fig. 1. The sampling nozzles were stainless steel tubes with an inner diameter of 4.0 mm. Both sample lines were made out of a 1/2 inch tube and they were approximately of the same length, which made the diffusion losses similar. Due to their placing in the laboratory the difference in the length of the lines was 6 cm. The sample lines were heated up to 200°C in order to avoid condensation and thermophoretic deposition before the diluter.

If the assumption of isokinetic sampling is considered, the optimal sample flow rate would be 2.56 l/min (NTP), as a 4 mm tube samples from 25 mm tube with 100 l/min (NTP) flow. If the sample flow is smaller than that, the particle concentration C_s of huge particles, $Stk > 1$, will be overestimated. For particles whose Stokes number is smaller than $Stk < 0.01$ the anisokinetic loss is negligible. TEOM measurements were done with 0.095 or 0.125 l/min (NTP) sample flow rates, so the sampling was anisokinetic. As the mass size distribution of particles does not change significantly in the heat exchanger, anisokinetic sampling has no effect on deposition results. In BLPI measurements the sample flow rate was 3.2 l/min (NTP) in Cu and 6.4 l/min (NTP) in NaCl experiment.

The sample flow had to be quenched for the aerosol measurements, because the instruments could not withstand high temperatures. For this reason, the sample flow was diluted with ambient nitrogen in a porous tube diluter, which prevented deposition during the quenching process (Auvinen, 1999). The dilution ratio was selected so that water would not condense into the tubes, even if they were not heated.

As the pressure in the system was constant, the sample flow rate and the dilution ratio could be controlled by adjusting the dilution flow. This was done with a mass flow controller.

2.3 Measuring instruments

2.3.1 Berner Low Pressure Impactor

The particle size distribution was measured with a Berner low pressure impactor (BLPI). It is an 11 stage cascade impactor, which is capable of classifying particles from 15.66 μm down to 0.0324 μm of diameter, because of the low pressure applied in the last stages (Hillamo and Kauppinen, 1991).

An impactor stage is composed of circular nozzles and a flat plate placed perpendicular to the flow path. Each impactor stage has a characteristic cut-off diameter D_{50} . Particles which have an aerodynamic diameter larger than the cut-off diameter can not follow the gas stream lines and be collected to the stage. In a cascade impactor smaller particles are passed on to the successive stages.

When the impactor stages are weighed after the collection, an aerosol mass size distribution based on the aerodynamic diameter of the particles is obtained.

The cut-off diameter, i.e., the diameter with 50% collection efficiency on the particular stage can be calculated with the following equation (Hinds 1999):

$$D_{50}\sqrt{C_c} = \left[\frac{9\mu D_j (Stk_{50})}{\rho_p U} \right]^{\frac{1}{2}}, \quad (1)$$

where $Stk_{50}=0.24$ for round nozzles or tubes. The cut-off diameters for BLPI have been experimentally determined in Hillamo and Kauppinen (1991). The results are comparable with the calculated cut-off

diameters.

2.3.2 TEOM 1400a

The Tapered Element Oscillating Microbalance (TEOM) is an aerosol mass monitoring device by Rupprecht and Pataschnick Co. In a TEOM the gas flows through an oscillating tapered element, which has a particle collection filter on the top. The TEOM monitors the changes of the element frequency and thus the mass collected to the filter on-line. The change of mass on the filter between two measurements is

$$dm = K \left(\frac{1}{f_2^2} - \frac{1}{f_1^2} \right), \quad (2)$$

where K is the spring constant of the oscillator. The frequency is around 250 Hz and the spring constant given by the manufacturer is 12516 kg/s² (Rupprecht and Pataschnick 1999). In the experiments the frequency was recorded every ten seconds. To decrease noise of calculated mass, two minute exponential averaging was used.

TEOM 1400a has a built-in mass flow controller, which allows the flow to be set between 0.5 and 5 l/min (NTP). In these experiments, a flow rate of 2.74 l/min (NTP) was selected. The gas flow was heated to 50°C in order to avoid condensation to the particles and to the filter. With this method the mass concentration of dry particles could be measured.

3 Experiments

3.1 Temperature and flow characteristics

Upon entering the heat exchanger, the temperature of the gas flow was measured to be 187-199°C depending on the gas mixture. The measured temperatures and characteristics of the main flow are presented in Table 1. In Table 2 are presented the temperatures of the cooling water when no particle deposition on the walls existed. The temperatures are averages from the experiments. Cooling water outlet temperature was measured from three points. One Pt100 detector and one T-type thermocouple were placed at two opposite outlets 3 cm after the heat exchanger. In the third measurement point was

also a T-type thermocouple and it was placed 10 cm after the four outlets were joined. In tables 2 and 5 the outlet temperature means the temperature measured from this third point where the water flow was mixed. In two other measurement points the temperature did not remain constant as the water flow rate through them fluctuated. The temperature variation is seen in appendix A figures 1 to 3.

Table 1. Temperature and gas flow characteristics in the heat exchanger.

Flow Inlet (NTP)		Flow Outlet (NTP)	T Inlet	T Outlet	Amount Condensed H ₂ O
N ₂ [l/min]	Steam [g/min]	[l/min]	[°C]	[°C]	[g/min]
100	-	100	199	125	-
75	18.4	86	190	127	7.2
25	60.5	46	187	149	39.4

Table 2. Temperature characteristics of the cooling water without aerosol deposition in the heat exchanger.

Flow Inlet (NTP)		Inlet T	Bottom T	Middle T	Top T	Outlets Mixed T
N ₂ [l/min]	Steam [g/min]	[°C]	[°C]	[°C]	[°C]	[°C]
100	-	29.3	29.5	29.7	30.0	31.9
75	18.4	29.1	29.9	30.6	31.4	35.5
25	60.5	29.6	31.7	35.1	41.3	52.3

With all gas compositions the flow Reynolds number at the heat exchanger inlet was approximately 4700. The condensation to the heat exchanger naturally increased, when there was more steam in the gas flow. Steam condensation led to a decreased flow rate and affected thus the Reynolds number of the flow. With pure nitrogen, the flow Reynolds number increased with decreasing temperature up to 5800 at the outlet of the heat exchanger. With the medium steam flow, the Reynolds number stayed approximately at a constant value of 4700. With the greatest steam mass fraction, the flow Reynolds number decreased to 2400. The gas temperature at the outlet of the heat exchanger was measured at the center of the flow channel. It increased with the increasing steam mass fraction from 116°C to 150°C, as presented in Table 1. The cooling water was flowing from the bottom to the top of the heat exchanger. The temperature of the 1.0 l/min cooling water flow was 29.5° at the inlet. The cooling water temperature at the outlet was 32°C with the pure nitrogen flow, 36°C with the medium steam flow and 52°C with the high steam flow. The energy balance in these temperature measurements is seen in table 3. The heat of gas at the outlet can not be exactly calculated, as the temperature gradient at the outlet is huge, and only the maximum temperature is measured.

Table 3. Energy balance in the heat exchanger.

Flow, Inlet (NTP)			$Q_{out}-Q_{in}$
N ₂ [l/min]	Steam [g/min]		[kJ /min]
100	-	Gas	-9.7
		Cooling water	11.1
75	18.4	Gas	-27.1
		Cooling water	26.5
25	60.5	Gas	-108.2
		Cooling water	94.9

3.2 Aerosol measurements

In total, eight deposition experiments were carried out with aerosol measuring instruments. The experimental matrix is presented in Table 4. In the first two experiments, the aerosol mass size distribution was studied using Berner low pressure impactors (BLPI). In both experiments two

impactor samples were taken from the heat exchanger inlet. The sampling times were between 1.5 and 5 minutes.

Table 4. The experimental matrix of aerosol deposition studies.

Exp.	Aerosol material	N ₂ flow [l/min] (NTP)	H ₂ O flow [mol/min]	H ₂ O / N ₂ Molar ratio	Measuring Instruments
1.	NaCl	100	-	0 / 100	BLPI
2.	Cu	100	-	0 / 100	BLPI
3.	NaCl	100	-	0 / 100	TEOM
4.	NaCl	75	1.02	23 / 75	TEOM
5.	NaCl	25	3.36	75 / 25	TEOM
6.	Cu	100	-	0 / 100	TEOM

After the size distribution measurements, a set of experiments was conducted using TEOM 1400a on-line mass monitor to measure the aerosol mass concentration. The deposition could be calculated from the concentration difference between the inlet and the outlet of the heat exchanger. In each experiment, eight to ten measurements were conducted by swapping the sampling between the heat exchanger inlet and outlet. The duration of one TEOM measurement was 11-15 minutes.

4 Results

4.1 Mass size distribution

From previous measurements it is known, that the particle mass size distributions measured with BLPI are not much affected by deposition. Thermophoresis depends on the particle size, but the thermophoretic deposition rate is so small, that the change in mass size distribution is insignificant. The mass size distributions of Cu and NaCl particles are presented in figure 2.

The aerodynamic mass median diameters (AMMD) of Cu and NaCl particles calculated from the distributions were $3.1 \mu\text{m}$ and $0.45 \mu\text{m}$ respectively. The geometric standard deviation was 1.65 for Cu and 1.53 for NaCl. Mass concentration in the experiments with NaCl varied between 200 and 450 mg/m^3 . Mass concentration of Cu was between 300 and 400 mg/m^3 .

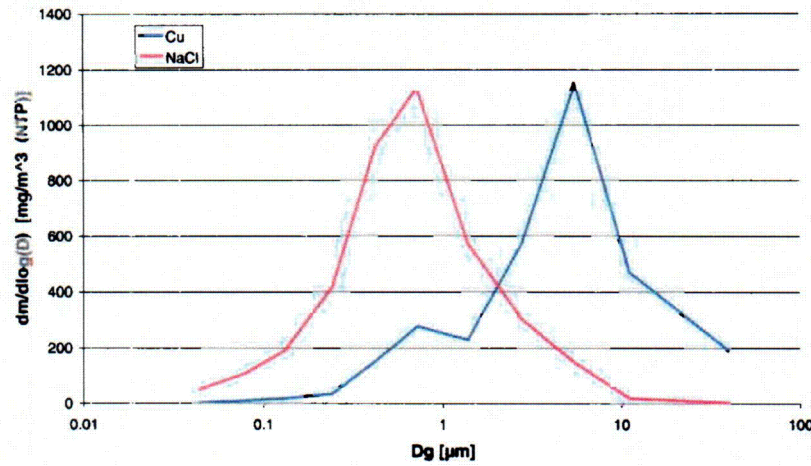


Figure 2. Aerosol mass size distributions of Cu and NaCl particles.

4.2 Deposition

The average percentage of deposited particulate mass in all four experiments, measured with TEOM1400a, is presented in Table 5.

Table 5. Average deposited mass in the heat exchanger tube, measured with TEOM.

Flow [l/min] (NTP)	Aerosol material	Deposition [%]
100 N ₂	Cu	2
100 N ₂	NaCl	2
23 H ₂ O + 75 N ₂	NaCl	12
75 H ₂ O + 25 N ₂	NaCl	64

With a 100 l/min (NTP) nitrogen flow the deposition to the heat exchanger was 2% of the particle mass. It can be concluded that the thermophoresis and turbulent impaction, which are the main deposition phenomena in dry gas flow, were relatively weak in these experiments. With the low water content flow, the deposition rate was significantly higher, in average 12% of the particle mass. This increase was caused by diffusiophoresis. As expected, the deposition rate increased further with the steam rich flow. On average, 64% of the NaCl particles deposited in the experiment.

The mass concentration of the particles increased during the experiments with steam. The reason for this is, that NaCl condensed and deposited on the tube wall after the furnace more in the beginning of the experiment. The tube between furnace and mixer was almost clogged after the experiment. The tube was relatively cold compared to the temperature of flow through the furnace, as the main flow through mixer was only less than 200°C. Other possibility is, that water condensed in the porous stainless steel mixer and caused a high pressure difference through it. That would have caused the main flow rate to decrease during the experiment. Although that should have been seen as change in temperatures of cooling water, but no such thing could be observed.

Table 6. Temperature characteristics of the cooling water in Cu and NaCl experiments.

Flow Inlet (NTP)		Aerosol material	Inlet T	Bottom T	Middle T	Top T	Outlets Mixed T
N ₂ [l/min]	Steam [g/min]		[°C]	[°C]	[°C]	[°C]	[°C]
100		Cu	29.6	29.9	30.1	30.4	32.3
100	-	NaCl	29.5	29.5	29.7	29.9	31.9
75	18.4	NaCl	29.5	30.4	31.2	32.2	36.5
25	60.5	NaCl	29.8	32.9	36.3	43.5	55.1

The measured mass concentrations from inlet and outlet are almost equal except at high steam conditions. As the water condenses the flow rate is much smaller at the outlet. So the deposition percentage is determined mainly by the reduction of flow rate due to steam condensation.

The inner tube of the heat exchanger was changed after every experiment. Visually only a small amount of deposited material could be observed in any of the tubes. It was concluded that in the dry experiments the deposition velocity was very small. In steam rich conditions it was obvious that the condensed water washed most of the deposited particles out of the tube. The condensed water forms a thin layer on the tube wall. Because of the water layer the particles may not even reach the wall.

From tables 2 and 6 can be seen, that deposition did not have much effect on heat transfer. As the cooling water flow rate was the same in all cases, the difference in heat transfer is directly proportional to temperature change of cooling water. Especially, the heat transfer did not decrease. The amount of deposited material was not large. Heat transfer depends on the wall surface area and the deposition increases it.

5 Discussion and conclusions

Aerosol deposition in a vertical heat exchanger tube was studied in three different flow environments with NaCl particles: dry, low steam and high steam conditions. The deposition of Cu particles was investigated in dry conditions. The aerosol mass size distribution was characterized with the Berner Low Pressure Impactor (BLPI). The deposited mass fraction was measured using the Tapered Element Oscillating Microbalance (TEOM) by measuring the aerosol mass concentration alternately from the heat exchanger inlet and outlet.

The TEOM measurements agree quite well with the earlier preliminary studies (Lehtinen). Thermophoretic deposition is smaller, as the temperature difference between cooling water and gas flow is smaller. Also the vapor condensation rates were slightly smaller as expected. The deposition rate in low steam conditions goes hand in hand with condensation rate but in high steam conditions the deposition rate was higher than in preliminary studies. The results of preliminary studies and these studies are compared in table 7.

Table 7. Comparison with preliminary studies. Results of preliminary studies are in parentheses.

Case	Temperature [°C] Inlet → Outlet	Water flow [g/min] Inlet → Condens.	Deposition [particle loss %]
100% N ₂	199 → 125 (205 → 116)		2 (4)
75% N ₂ 25% H ₂ O	190 → 127 (207 → 129)	18.4 → 7.2 (→ 9.5)	12 (17)
25% N ₂ 75% H ₂ O	187 → 149 (203 → 150)	60.5 → 39.4 (→ 43.3)	64 (53)

The amount of deposited material in the heat exchanger is small in all cases as the particles are flushed away with the condensed water or do not even reach the tube wall because of the thin water layer on the tube. Thus sticky deposit that decreases heat transfer and may cause blockage of the tube did not

form in these experiments. The aerosol mass was from 300 to 400 mg/m³ with copper and from 300 to 900 mg/m³ with NaCl. The effect of deposition to heat transfer was small.

7 References

A. Auvinen, "Fissionuotteiden uudelleenhöyrystymisen tutkimuslaitteisto", Master's Thesis, Helsinki University of Technology (1999), Department of Engineering Physics and Mathematics.

A. Dehbi, D. Suckow and S. Guentay, "AIDA Experiments: Aerosol Impact on the Performance of the SBWR Passive Containment Condenser Model", *ALPHA 711, TM-49-AIDA-1-97*, Paul Scherrer Institute (1997).

S. Guentay and D. Suckow, "ESBWR Passive Aerosol Removal – Maintaining Plant Simplicity for Offsite Dose Reduction", *TOPNUX 96 Economic Nuclear Power for the 21st century*, p. 629-640 (1996).

R. Hillamo and E. Kauppinen, "On the Performance of the Berner Low Pressure Impactor", *Aerosol Sci. Technol.*, Vol 14, p.33-47 (1991).

W. Hinds, *Aerosol Technology* 2nd edition, Wiley-Interscience (1999).

K. Lehtinen, J. Hokkinen, A. Auvinen, J. Jokiniemi and R. Gamble, "Studies on Steam Condensation and Particle Diffusiophoresis in a Heat Exchanger Tube", submitted to *Nucl. Eng. And Design*.

B.A. Posta and A.S.Rao, "European Simplified Boiling Water Reactor (ESBWR Plant)", *4th Int. Conf. Of Nucl. Eng.*, New Orleans, LA, USA (1996).

Rupprecht & Pataschnick Co. Inc, TEOM 1400A Instruction Manual (1999).

A. Watanabe, K. Nemoto, M. Akinaga and H. Oikawa, "Insoluble Aerosol Behavior Inside the PCCS Condenser Tube Under Severe Accident Conditions", *International Conference on Nuclear Engineering*, Vol. 2, ASME (1996).

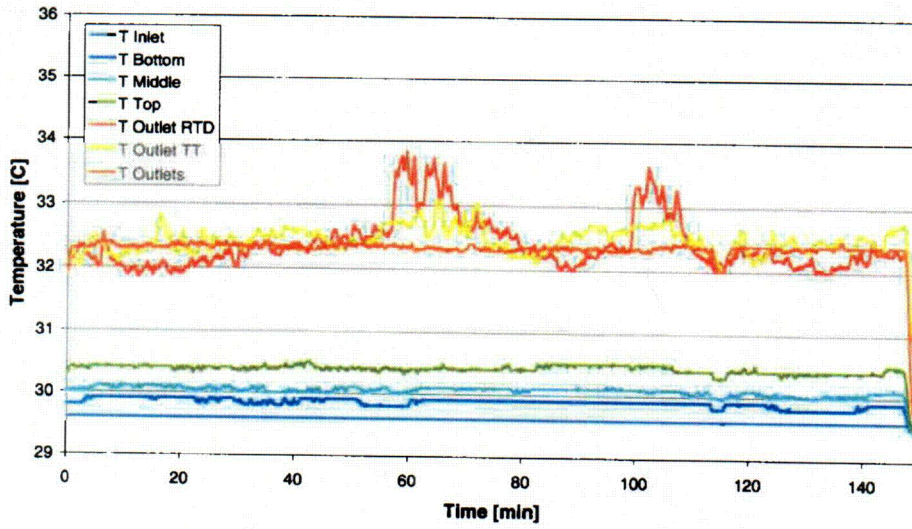
Appendices

Appendix A Temperature measurement data

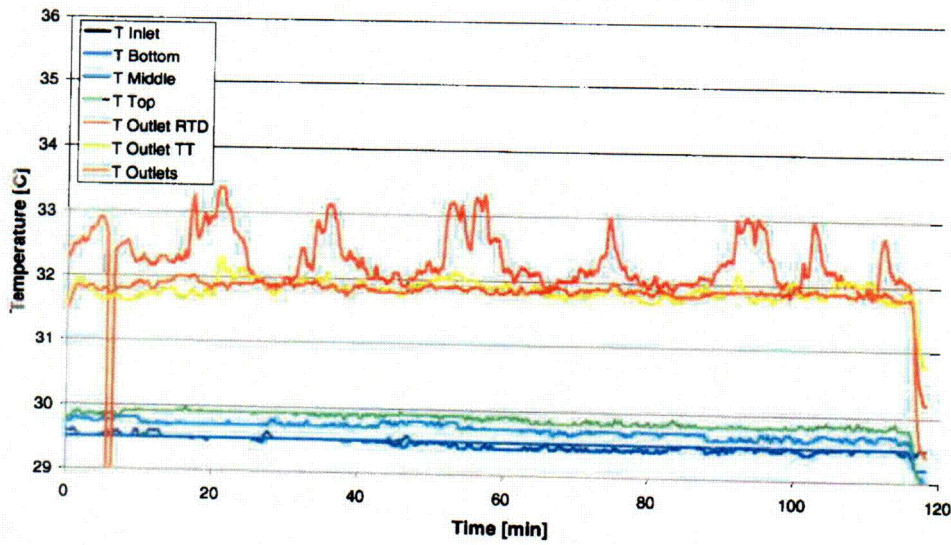
Appendix B TEOM measurement data

Appendix A

Temperatures in 100 l/min (NTP) N₂ / Cu experiment

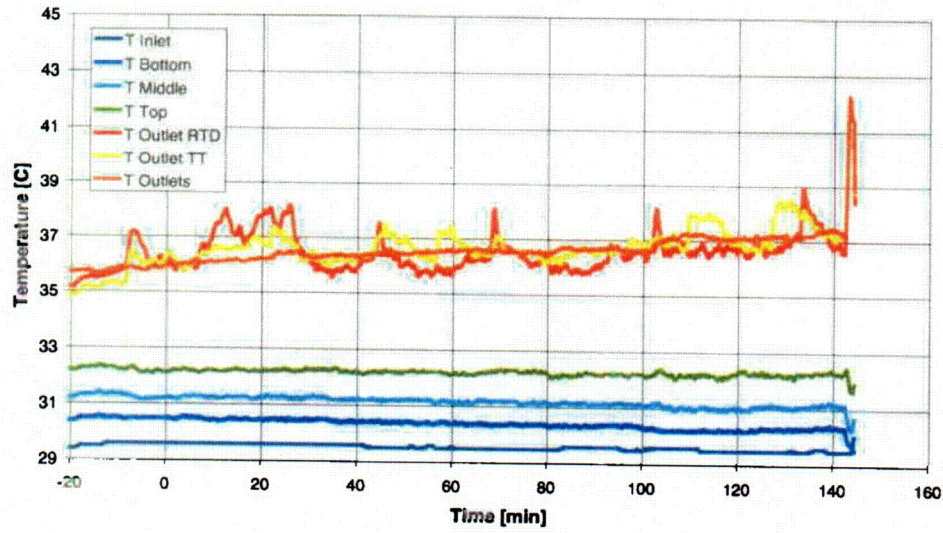


Temperatures in 100 Nlpm N₂ / NaCl experiment

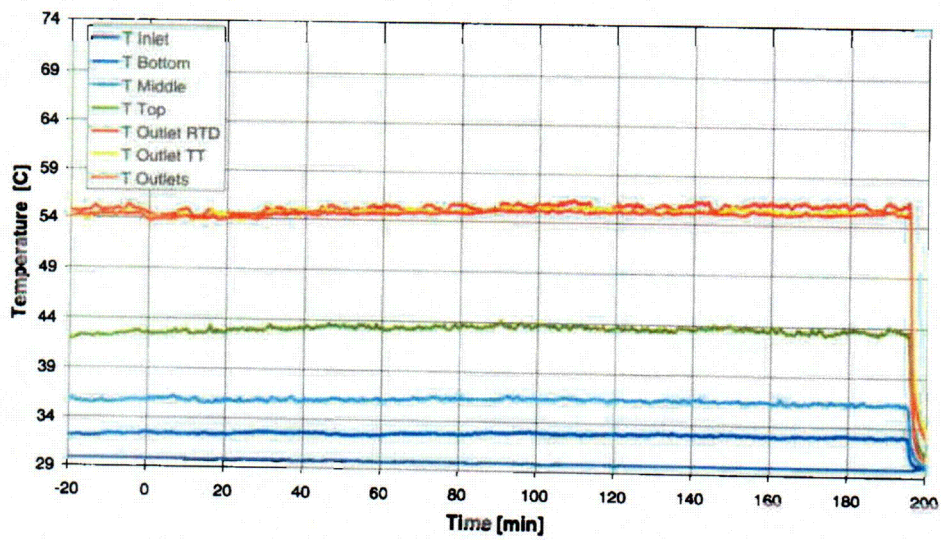


Appendix A

Temperatures in 25 l/min H₂O + 75 l/min N₂ / NaCl experiment

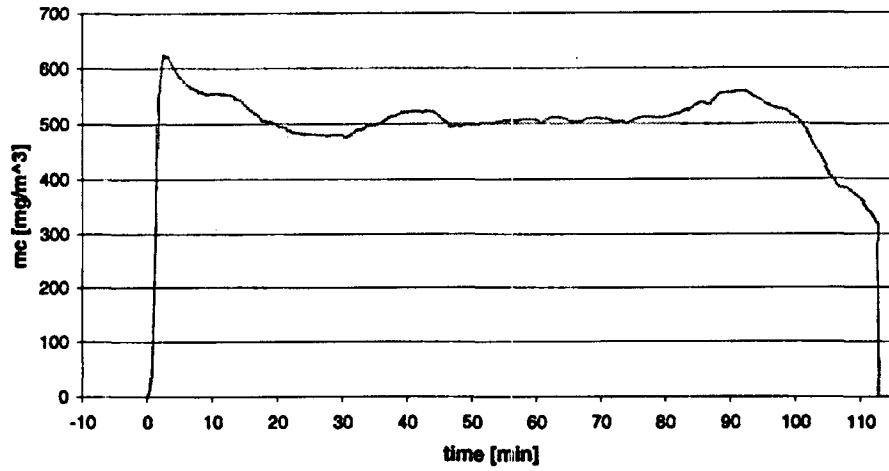


Temperatures in 75 l/min H₂O + 25 l/min N₂ / NaCl experiment

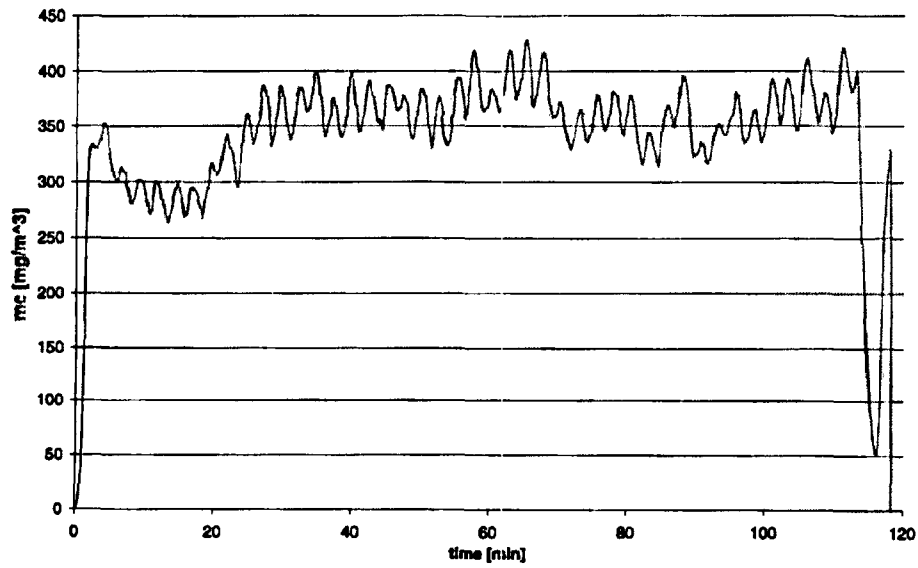


Appendix B

NaCl Mass Concentration, Gas flow 100 l/min N2

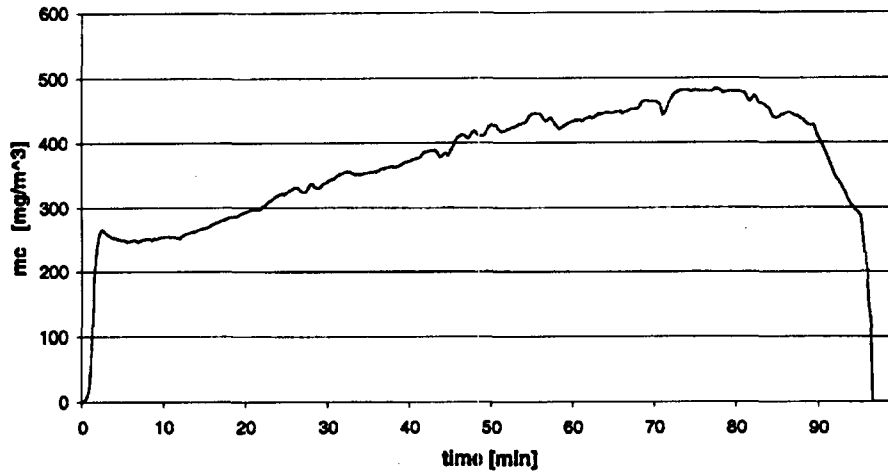


Cu Mass Concentration, Gas flow 100 l/min N2

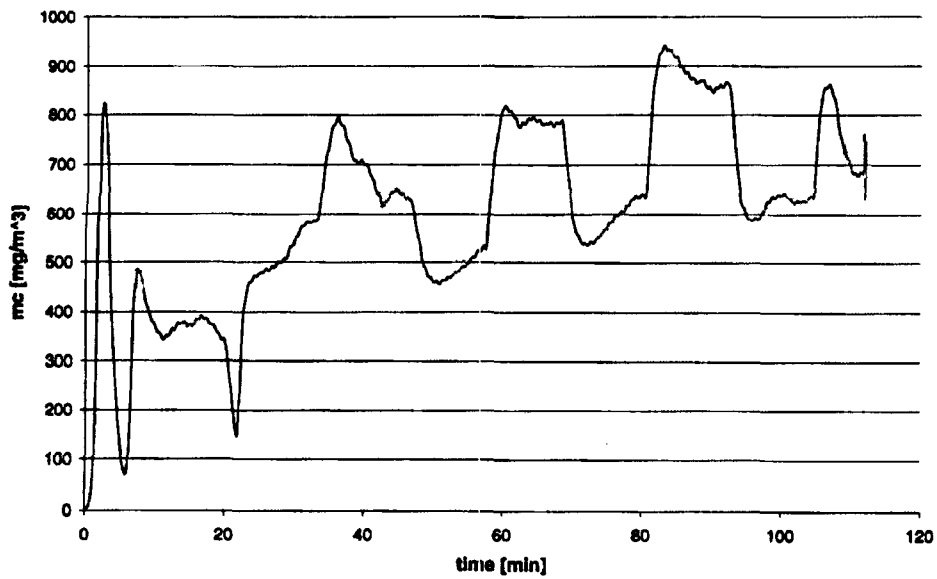


Appendix B

NaCl Mass Concentration, gas flow 23 l/min H₂O + 75 l/min N₂



NaCl Mass Concentration, Gas flow 75 l/min H₂O + 25 l/min N₂



Part II Radiotracer experiments

1. Introduction

The experiments with aerosol equipment have focused on solving the particle deposition mechanisms into a vertical heat exchanger tube in different conditions. These studies have been important in understanding the behavior of the heat exchanger in a severe accident. However, the final objective of the study is to resolve the effect of aerosol deposition on the capacity of the heat exchanger. In order to do that, it is not enough to know just the aerosol deposition rate. It is as important to know the removal rate of the deposited material.

The accumulation of the deposited material is measured by adding a radiotracer into the aerosol and applying sequential scintillation detectors. With this method the possible downward movement of the deposited particles can be verified. The absolute amount of deposited material can be calculated in real time by comparing the measured activities to the total activity of the sample. The fraction of aerosol deposited into the heat exchanger tube can also be estimated, since the activity of the filter is monitored during the experiment. When the data obtained from the activity measurements is compared to the simultaneously conducted temperature measurements, the effect of aerosol deposition on the performance of the heat exchanger can be solved.

2. Requirements for the aerosol material

The behavior of the heat exchanger is studied in the presence of two different kinds of aerosol. One of the materials is water-soluble and the other is insoluble. In the previous study cesium hydroxide and silver were applied for aerosol production. Materials that are chosen for the present work should have similar behavior.

It is important to be able to produce a relatively high mass concentration of particles, because the objective is to measure the effect of deposition on the heat transfer. For the same reason, the production rate has to be very stable. One of the materials should have aerodynamic mass median diameter of the particles close to 1 μm , so that the results can be compared with the previous study. In order to verify the influence of other important deposition mechanisms (especially turbulent eddy impaction), the other aerosol material should have a larger particle size. The chosen materials may not react chemically with each other or with the tube surface. Neither may they form gaseous compounds in the experimental conditions. Furthermore, the materials must be readily available in a reasonable price.

For the radiotracer experiments, the materials have to be activated in a nuclear reactor. The produced radioactive isotope must have a relatively short half-life (less than 20 hours), so that the used equipment can be easily disposed. For the same reason, the activated isotope may not have long lived daughter nuclides and the level of impurities in the material must be low. In order to avoid excess activity, a high-energy gamma has to be produced in a significant fraction of the decays. It is also beneficial, if the gamma rays coming from different aerosol materials can be easily separated.

There are very few materials that fulfil all these requirements. Two candidates considered for the soluble material are sodium- and potassium chloride. The behavior of both alkaline is similar to cesium and they can be activated easily into a suitable short-lived isotope. The half-life of ^{24}Na and ^{42}K are 14.959 h and 12.36 h respectively. The biggest problem with potassium is its natural long lived ($T_{1/2} = 1.27\text{E}9$ y) radioactive isotope ^{40}K . A small amount of this isotope would also be formed during the

activation. Another problem is that only 18% of the ^{42}K decays cause a characteristic 1525 keV γ -ray. This means that the level of activity must be relatively high. All decays of ^{24}Na yield a characteristic 1369 keV γ -ray. The difficulty with sodium is that almost all decays (99.94%) also yield a 2754 keV γ -ray. This will increase the dose of the laboratory personnel, because it is practically impossible to shield such a high-energy gamma. As yet it is not decided, which material will be applied in the production of soluble aerosol. Sodium chloride is the probable choice though, since it was already used in the inactive experiments.

The only alternative for insoluble material, which fulfilled all the requirements was copper. The active isotope, ^{64}Cu , has a suitable half-life of 12.7 h. It has only a very weak, 0.47%, characteristic gamma peak at 1346 keV. However, 61% of ^{64}Cu decays result a positron and thus an annihilation gamma. A very wide range of different copper powders is commercially available. The powder applied in the radio tracer studies was also used in the production of the inactive aerosol.

3. Experimental set-up

Basically, the system used in the first radio tracer experiment remained the same as in the inactive experiments. The modifications included removing all aerosol measurement equipment and sampling lines and adding filtration to the outlet of the system. The only significant difference in the experimental line was the heating band wrapped around the flow mixer.

The accumulation of the aerosol into the heat exchanger is measured with five sequentially placed scintillation detectors. The sixth scintillation detector and a germanium detector are measuring the activity collected into the filter. The absolute amount of deposited material can be estimated by measuring the total activity of the sample before the experiment. This value has to be corrected with the self-absorption to the sample. The fraction of deposited aerosol is estimated by comparing the results of the sequential detectors to the data obtained with the filter detector. The estimate will inevitably have a small systematic error due to the different geometry between the tube and the filter.

In order to ensure an invariable measuring geometry, the sequential detectors, lead shielding and the heat exchanger are all attached to a supporting frame. The rack is designed in such a way that each detector will have an unobstructed view over a 17 cm long section of the tube. Together the detectors can thus cover 85 cm, which is the cooled length of the heat exchanger. The lead bricks are placed on slanted shelves so that the view of the detectors will be restricted effectively. The size of the lead bricks also mainly determines the dimensions of the frame. The distance from the centerline of the heat exchanger tube to the surface of the detectors is 350 mm. The detectors measuring the filter are placed at the same distance from its center. A relatively long distance is required in order to decrease the geometrical error. A photograph of the detector set-up is presented in figure II.1.

During the first radiotracer experiments some disturbances were observed in the flow of the coolant water. In order to stabilize the flow, several modifications were completed to the cooling system. Firstly, the number of water outlets was reduced from four to two. The outlet lines were also rearranged so, that the temperature detectors would always stay submerged. Secondly, the water reservoir was placed below the heat exchanger inlet and the siphon system was completely removed. The water pumped to the heat exchanger can thus flow freely down to the drainage. However, the most important modification was to drill air holes on top of the heat exchanger and to the highest point of the coolant line. Air bubbles will therefore no longer disturb the flow of the coolant.

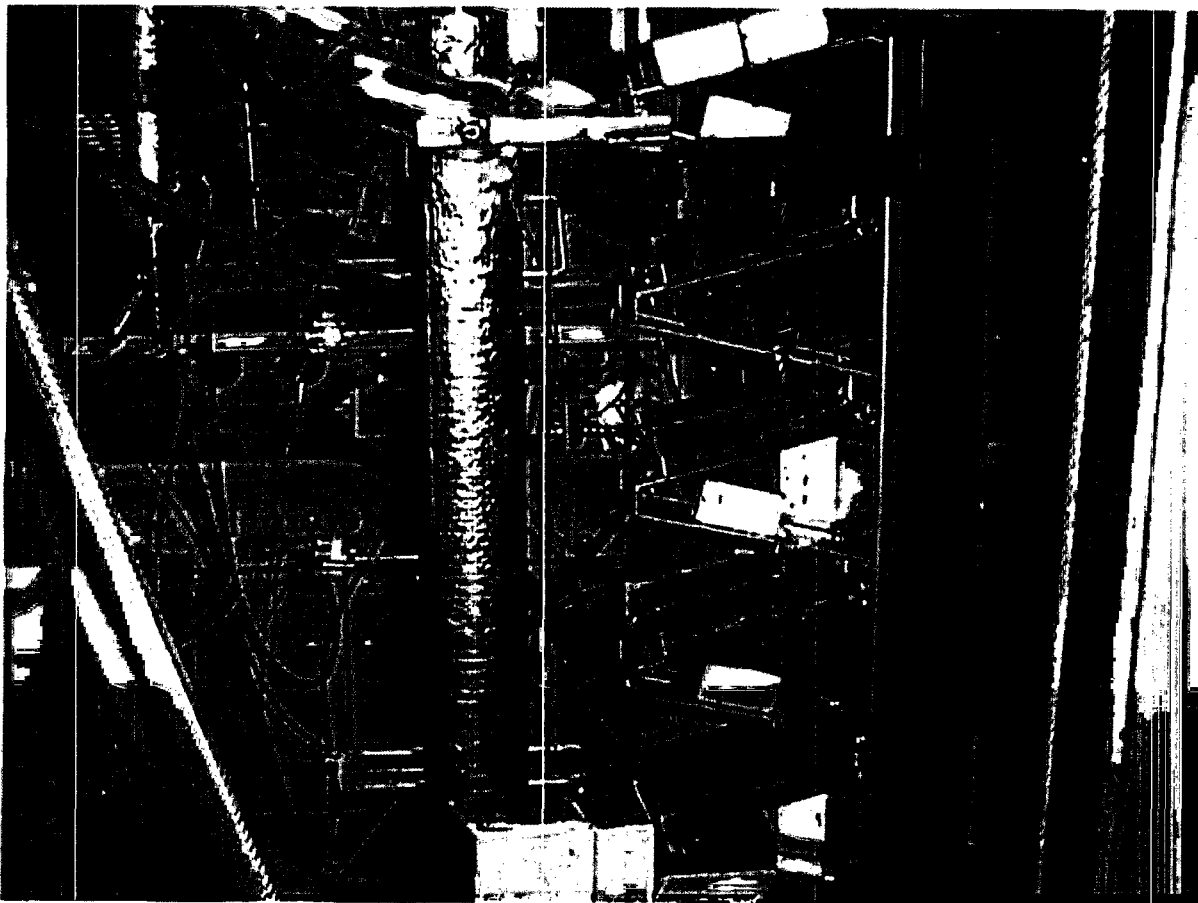


Figure II.1 Detector set-up for the radiotracer experiments.

4. Calibration of the sequential detectors

The calibration of the sequential detectors is a five-step process. The first thing to be corrected is the background noise. This can simply be done by measuring the level of the noise with each detector. The second step is to perform an efficiency calibration. The pulse rate coming from a standard calibration source has to be measured with all detectors, because each scintillation detector has a different sensitivity to radiation. Thirdly, the decay rate of the sample has to be taken into account especially, when short-lived isotopes are applied in the experiments. There is also a need to complete an energy calibration, if several radionuclides are to be measured. Scintillation detectors can not measure the energy of the gamma, but their sensitivity decreases, when the energy of a γ -ray increases. This energy efficiency function is unique for each detector. So, a proper energy calibration has to be done with monoenergetic sources. The gamma energies from these sources should be close to those, which will be measured in the experiments. Lastly, the effect of the lead shielding has to be taken into account, because the objective of the experiments is to measure the deposition profile in a tube.

The detector set-up was calibrated with a copper sample placed into the centerline of the heat exchanger tube. The sample was measured simultaneously with all detectors at one position for 30 seconds. After the measurement, it was moved one centimeter along the tube. With 101 measurements the whole length of the heat exchanger tube was covered. The result from the measurement is presented in figure II.2. In the figure, x-axis is the position of the calibration sample ($x = 0$ is the outlet

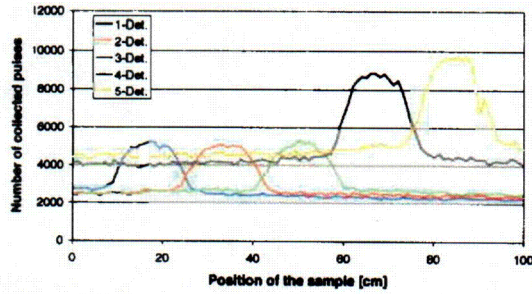


Figure II.2 Measured number of pulses with copper sample.

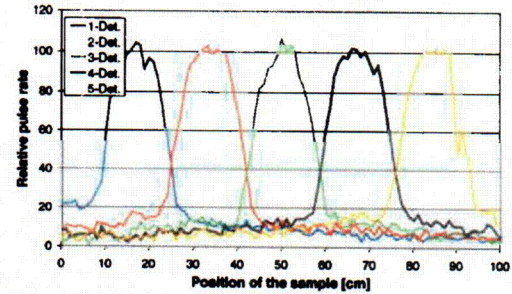


Figure II.3 Corrected pulse rate with copper sample.

of the tube) and y-axis is the number of collected pulses. The different background and efficiency of the detectors is clearly evident from the figure.

When the sample was directly in front of the detector, the measurement was applied as the efficiency calibration. Since the collection time was rather short, the calibration was not very accurate. However, for the testing of the system the accuracy was reasonable. The corrected result from the measurement is presented in figure II.3. The result is scaled to 100%, which will also be the case, when an aerosol sample is measured. There is no need for energy calibration in the preliminary experiment, since only copper is applied as aerosol material.

The effect of lead shielding can be estimated from the previous result. Presenting the detected activity as a function of distance from the centerline of the detector does it. The following combination of three fourth order polynomials are applied as a shielding function,

$$S(x) = k_1 \times P_1(x) + k_2 \times P_2(x) + k_3 \times P_3(x) \quad (\text{II.1})$$

where k_i 's are step-functions of the form:

$$k_1 = \frac{1}{1 + \exp\left(\frac{x - a_1}{b_1}\right)} \quad (\text{II.2})$$

$$k_2 = \frac{1}{1 + \exp\left(\frac{x - a_3}{b_3}\right)} - \frac{1}{1 + \exp\left(\frac{x - a_2}{b_2}\right)} \quad (\text{II.3})$$

$$k_3 = 1 - \frac{1}{1 + \exp\left(\frac{x - a_4}{b_4}\right)} \quad (\text{II.4})$$

Here parameters a_i indicate the place and parameters b_i the steepness of the step. Parameters of the step functions and polynomials are presented in table II.1. The fitted function is presented together with the data points in figure II.4.

i	a	b	α_1	α_2	α_3
1.	-7.7925	0.036271	22.5477	103.4888	30.6621
2.	-8.3690	0.66871	0.5299	1.1061	-1.6898
3.	9.4581	0.41591	-1.6403E-3	-0.8738	4.7731E-2
4.	9.1868	0.024854	-1.7487E-4	-2.0174E-3	-6.1658E-4
5.			-1.3194E-6	-1.5649E-5	2.9104E-6

Table II.1 Parameters for the shielding function, $S(x)$.

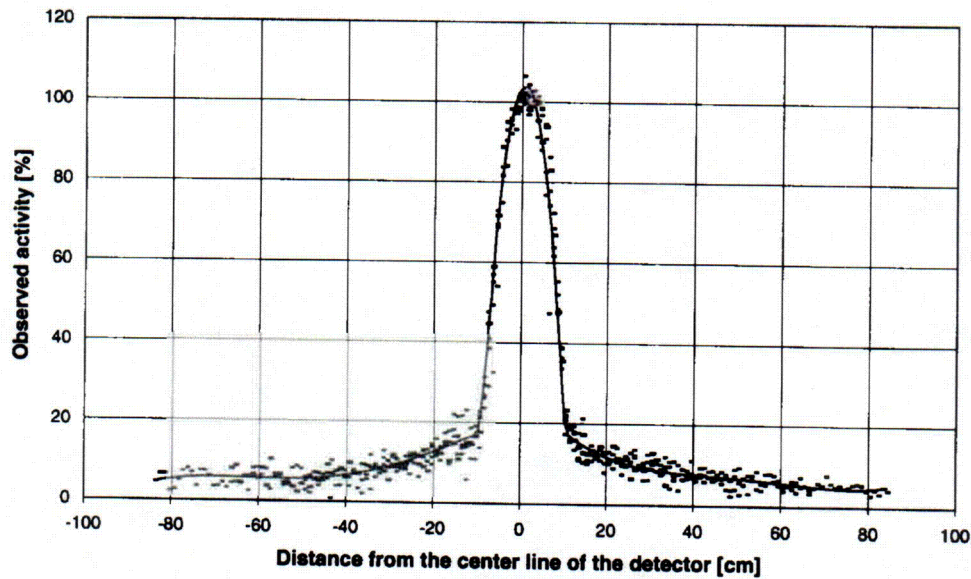


Figure II.4 Shielding function, $S(x)$, for copper measurements.

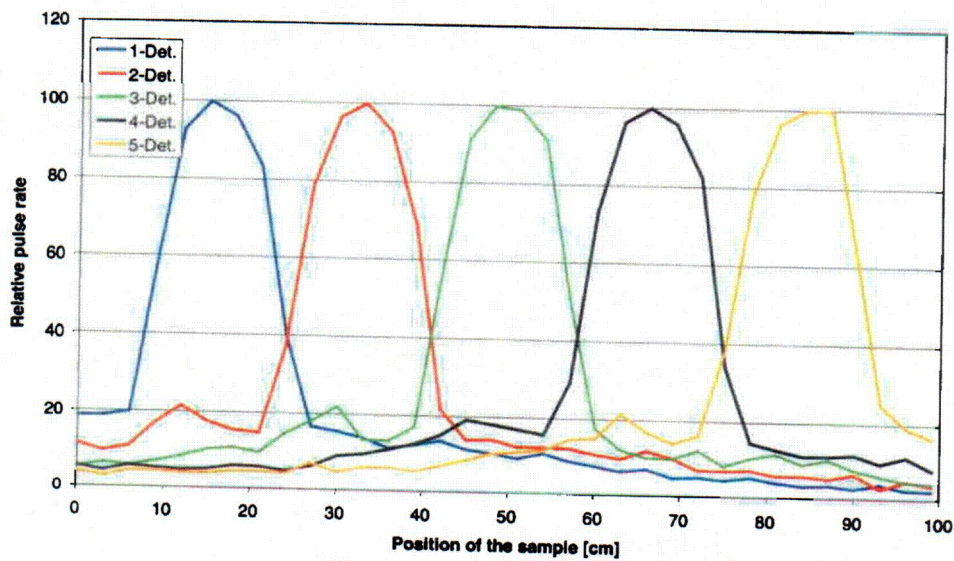


Figure II.5 Corrected pulse rate with cobalt sample.

Similar measurements were conducted using a cobalt calibration sample. ^{60}Co emits characteristic γ -rays at energies of 1173 keV (99.90%) and 1333 keV (99.982%), which are close to the gamma energies from sodium and potassium. Unlike previous experiment the sample was moved three centimeters between the measurements. The corrected results are presented in figure II.5. The asymmetric nature of the lead shielding can be seen clearly from the figure. There is a second maximum at the relative pulse rate approximately 20 centimeters downstream the center of the detector. This could not be seen with the copper sample, because the annihilation gamma could not penetrate so well through the lead shielding.

5. Preliminary experiment

One preliminary experiment with active copper aerosol was conducted at the end of the year. The purpose of the experiment was to test the performance of the facility and to complete the validation of the experimental procedures. After the experiment also mathematical tools could be developed for data analysis.

The conditions in the preliminary experiment were exactly the same as in the dry inactive experiments. The nitrogen flow rate was 100 l/min (NTP), of which 20 l/min was directed through the aerosol generator. The temperature of the gas was 200°C at the inlet of the heat exchanger. The aerosol was produced from copper powder using a dry powder generator. The flow rate of the coolant water was 1 l/min and the inlet temperature was 30°C. The gas and coolant flows were switched on long before the experiment in order to stabilize the temperatures in the system. The activity measurements were started five minutes before the aerosol feed. Each measurement lasted for 30 seconds and the duration of all measurements was 60 minutes.

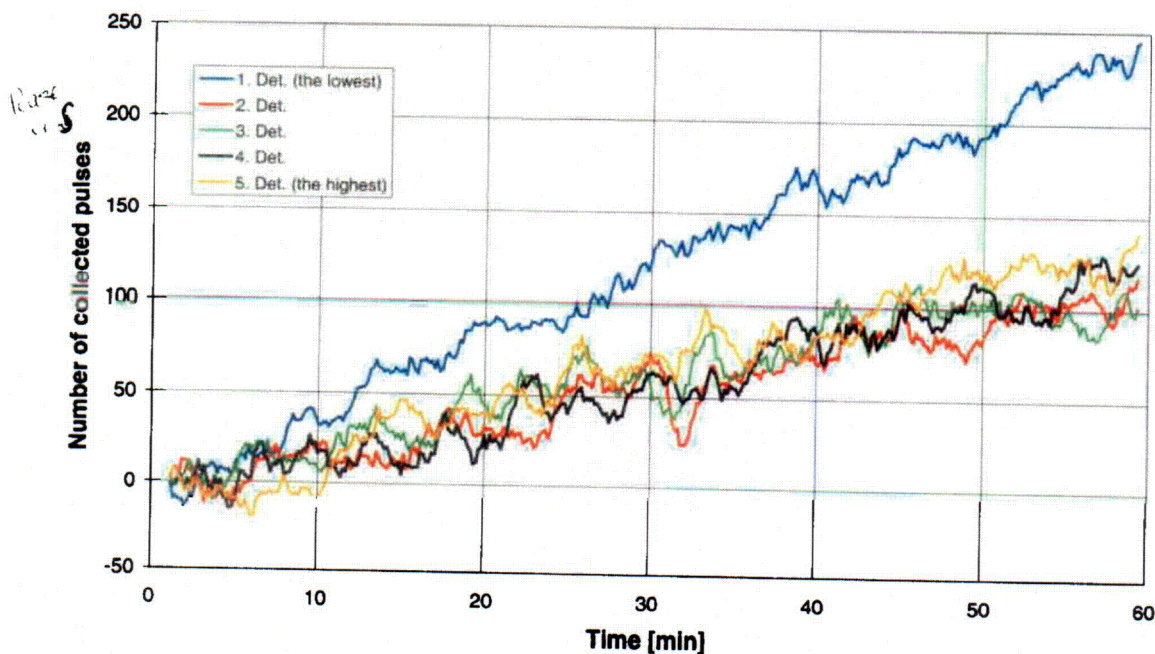


Figure II.6 The averaged number of pulses collected in the preliminary experiment.

The number of pulses collected with detectors during each 30 second measurement is presented in figure II.6. The activity used in the preliminary experiment was very low, which resulted a poor statistical accuracy. Therefore the data presented in the figure is averaged. It is still obvious that the amount of copper in the tube was steadily increasing throughout the experiment. The pulse rate measured with the detector, which was located near the outlet of the tube, was increasing more rapidly than the others were. All the other detectors gave almost identical readings. There is a possibility that the higher pulse rate with the outlet detector is due to its close proximity to the filter. Even though the detectors measuring the tube are well shielded from the filter, some pulses penetrate always through the shielding. This can lead to a significant error in deposition measurements, because the activity collected into the filter is much higher than what is deposited into the tube. The effect of filter deposit can be corrected by placing the sample into the position of the filter before the next experiment.

The deposition profile in the heat exchanger was estimated from the data using the shielding function. The accumulation of the deposit into the 85 cm long cooled section is presented in figure II.7. Again, the deposition into the outlet may be overestimated, because the pulses coming from the filter are not taken into account. For the same reason, deposition between 60 and 70 cm may be underestimated.

The temperature of the coolant water during the experiment is presented in figure II.8. The temperature measurements began 20 minutes before the activity measurements and lasted throughout the experiment. It is evident from the figure that the aerosol deposition did not have a noticeable effect on the temperature of the coolant. Obviously a thin copper deposit did not decrease the heat transfer in dry conditions. The effect of flow disturbances at the outlet can also be seen in the figure. This lead to modifications of the coolant system as described in chapter 3.

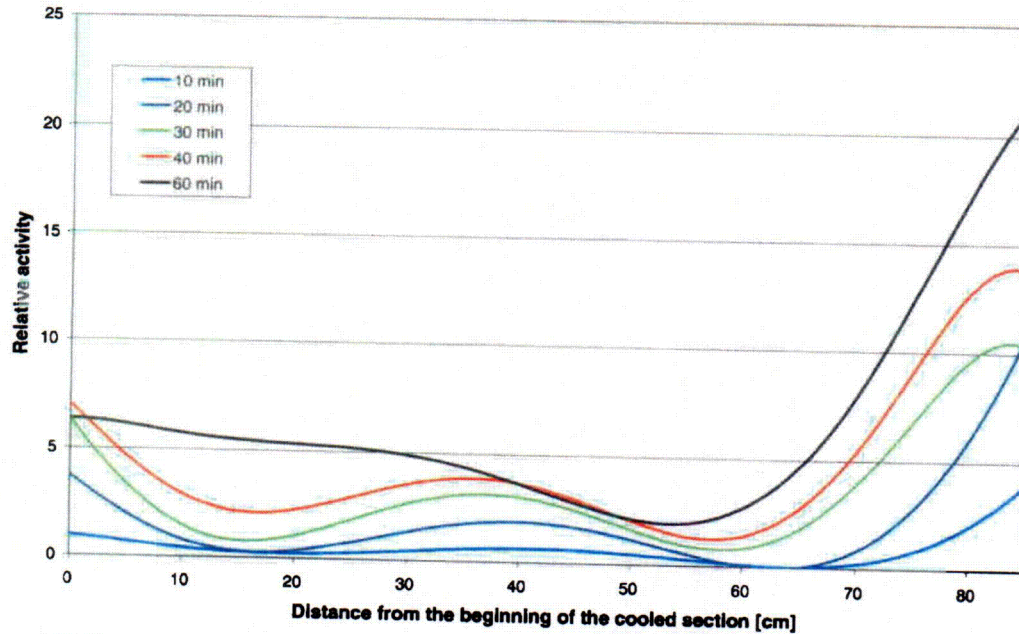


Figure II.7 The accumulation of copper into the cooled section of the tube in the preliminary experiment.

In the coming experiments, there is still a need to do a proper efficiency calibration. This is especially needed for the filter detector, which was not calibrated at all for the preliminary experiment. When this is done, the fraction of aerosol deposited into the tube can be calculated also in the preliminary experiment.

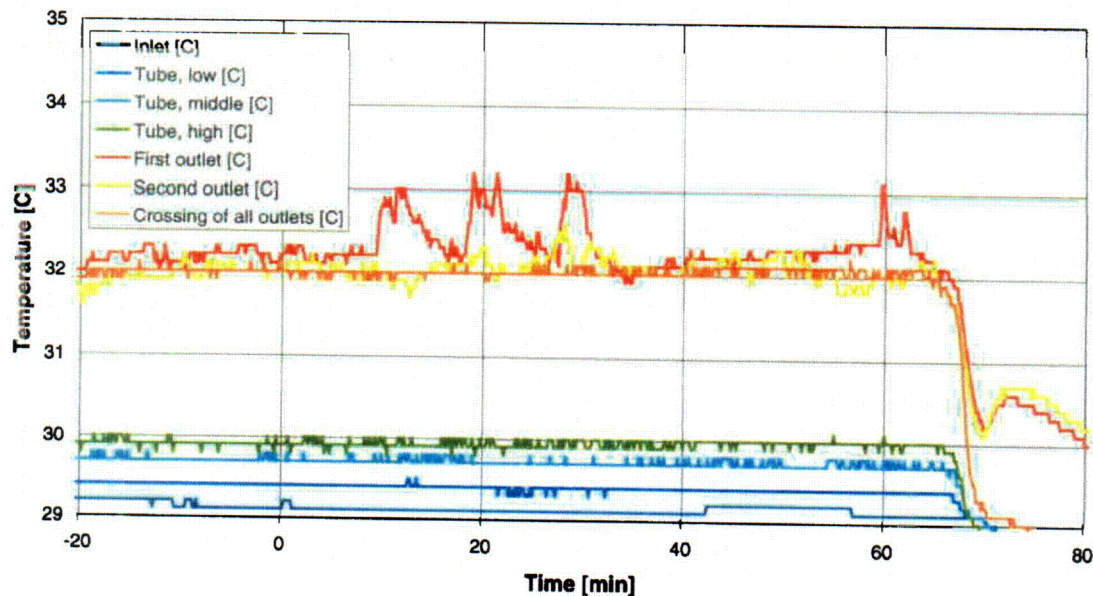


Figure II.8 Cooling water temperatures during the preliminary experiment.

6. Conclusions

The preliminary experiment confirmed that the accumulation of deposited aerosol could be measured in real time. The performance of the system was reliable. The temperature measurements were accurate enough, so that the effect of deposited aerosol on the heat transfer can be observed. A major achievement was also to develop data analysis, which can be applied in the future experiments.

The preliminary experiment also proved that deposited copper particles did not have a noticeable effect on the heat transfer in dry conditions. The situation may be different, when the aerosol is changed to a material, which does not conduct heat so well. The significance of aerosol deposition may also be greater in condensing conditions. Especially, when the temperature of the cooling water is higher, even a small difference in temperature may result a very significant change in the condensation rate.

One of the most important tasks remaining is to develop a meaningful test matrix for the future experiments. The experimental conditions should be chosen so that the effect of aerosol deposition is clearly evident from the results. The conditions should also be relevant for the passive containment condenser. An interesting and poorly understood phenomenon, which could be measured with the current test system, is the removal of deposited material by condensed water. Because the removal may be very significant for the performance of PCC, some experiments should focus on it. And lastly, the experiments should be conducted so that the result can be applied in the validation of the condensation model developed for Fluent. This would ensure that the results could be scaled up.

Part III Surface Steam Condensation in Computational Fluid Dynamics

Condensation is a phenomenon in which phase change, mass and heat transfer take place. We focus our interest on surface condensation, which occurs when the temperature of the water vapour is reduced below its saturation temperature. In industrial equipment, the process commonly results from contact between the water vapour and a cool surface. The latent energy of the water vapour is released, heat is transferred to the surface and a condensate is formed. Condensation may occur in one of two ways depending on the conditions of the surface. The dominant form of condensation is one in which a liquid film covers the entire condensing surface, and under the action of gravity the film flows continuously from the surface. Film condensation is characteristic of clean, uncontaminated surfaces. However, if the surface is coated with a substance that inhibits wetting, it is possible to maintain dropwise condensation. Regardless of its form, the condensate provides a resistance to heat transfer between the water vapour and the surface. This resistance increases with condensate thickness, which increases in the flow direction. We concentrate on film condensation, as this one mainly occurs in condensation inside a vertical tube.

Condensation is not only determined by the heat transfer through the condensate, but also through the wall and into the coolant, e.g. the cooling water. A schematic of the heat transfer is shown in Figure 1, where q are the corresponding heat fluxes and T the temperatures. In steady state conditions there is no storage of heat and all the heat that enters eventually exits. Based on that the heat fluxes can be equalised. Heat is transferred from the gas phase by convection, q_{conv} , and the release of the latent heat due to the phase change, q_{cond} . The sum of these fluxes is equal to the sum of the flux traversing the liquid film $q_{lf,rad}$ and the effect of advection in the film $q_{lf,ax}$. The flux through the wall, q_{wall} , is equal to the fluxes entering from the film, $q_{lf,rad}$, and exiting to the cooling water, q_{cool-w} . The governing equations are the following

$$q_{cond} + q_{conv} = q_{lf,rad} + q_{lf,ax} \quad (1)$$

$$q_{lf,rad} = q_{wall} = q_{cool-w} \quad (2)$$

where the individual heat fluxes are

$$q_{conv} = h_{gas} \cdot (T_{gas} - T_{interf.}) \quad (3a)$$

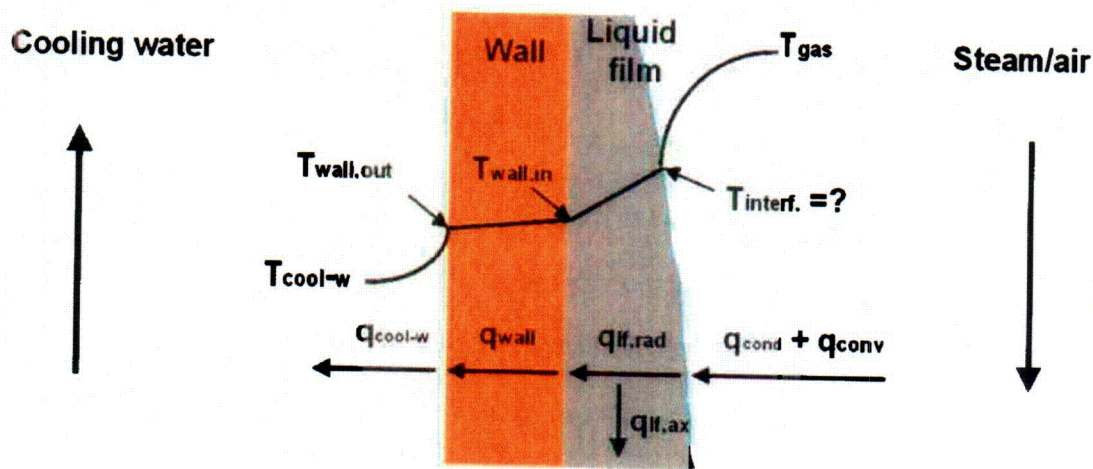


Fig. 1 Schematic of heat transfer with corresponding heat fluxes q and temperatures T . ($T_{interf.}$ corresponds to T_{inf} in the text)

$$q_{cond} = l \cdot \dot{m}_{cond} \quad (3b)$$

$$q_{lf,rad} = h_{lf} \cdot (T_{inf} - T_{wall,in}) \quad (3c)$$

$$q_{lf,ax} = F(Re, T_{inf}, T_{wall,in}) \quad (3d)$$

$$q_{wall} = h_{wall} \cdot (T_{wall,in} - T_{wall,out}) \quad (3e)$$

$$q_{cool-w} = h_{cool-w} \cdot (T_{wall,out} - T_{cool-w}) \quad (3f)$$

The heat transfer coefficient in different media are h_{xx} (W/m²K), the latent heat l (J/kg) and the condensed mass \dot{m}_{cond} (kg/sm²). At this stage in our approach to model condensation we do not consider heat transfer by advection in the liquid film and neglect Eq. 3d. Therefore Eq.1 becomes

$$q_{cond} + q_{conv} = q_{lf,rad} \quad (1b)$$

The heat transfer coefficients h_{gas} and h_{cool-w} are average quantities, which depend on the flow conditions and properties in the gas and the cooling water, respectively. In Equations 3, T_{inf} is the temperature of the interface between the gas and the liquid film where condensation takes place. This interface is in thermodynamic equilibrium, i.e. as many vapour molecules enter the liquid from the gas phase, as escape from the liquid to the gas. This means that the saturated vapour pressure at the interface of the liquid equals that of the gas (or in case of a gas mixture, the partial pressure of the vapour). The saturated vapour pressure, P_{sat} , is a function of temperature only and is shown in Figure 2. It can be seen that P_{sat} is extremely sensitive to increasing temperature. For a gas mixture of steam and a non-condensable gas the condensed mass in Eq. 3b will be explained briefly. It depends on $P_{sat}(T_{inf})$, the saturated vapour pressure at the interface, P_{vap} , the vapour pressure in the gas, P , the total pressure and the local properties of the gas flow in the following way

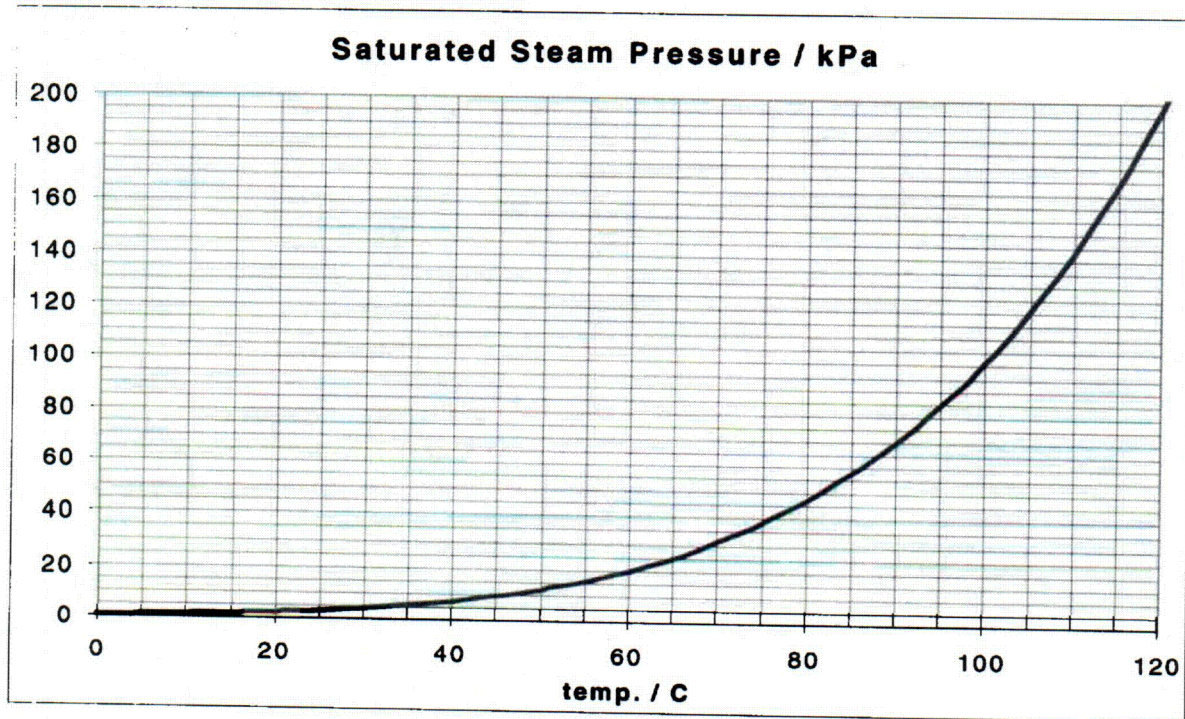


Fig.2 Saturated water vapour pressure (kPa) as a function of temperature (°C)

$$\dot{m}_{cond} = M_{vap} \cdot \frac{P_{tot}}{R \cdot T_{g,sat}} k \cdot \ln \frac{P_{tot} - P_{sat}(T_{int})}{P_{tot} - P_{sat}(T_{g,sat})} \quad (4)$$

where M_{vap} is the molecular weight of vapour, R the universal gas constant and

$$k = \frac{h_{gas}}{\rho c_p} Le^{0.67} \quad (5)$$

using ρc_p , consisting of the sum of the products of density and specific heat of the non condensable gas, nc, and the vapour, vap

$$\rho c_p = \rho_{nc} c_{p,nc} + \rho_{vap} c_{p,vap} \quad (6)$$

Le is the Lewis number

$$Le = \frac{D \cdot \rho c_p}{\lambda} \quad (7)$$

D is the binary diffusion coefficient and λ the thermal conductivity. These properties have to be evaluated at the saturation temperature equivalent to the vapour pressure in the gas ($T_{g,sat}$). Thus, condensation also is extremely sensitive to the interface temperature. The latent heat, l , also depends on this temperature.

In Eq. 3c the heat transfer coefficient of the liquid film is a function of Re_{lf} , its Reynolds number. Re_{lf} itself is a function of the condensate flow rate, which on the other hand depends on condensation

$$Re_{lf} = \frac{4\dot{m}_{cond}}{\mu_{lf} \cdot b} \quad (8)$$

μ_{lf} is the film viscosity and b the width of condensing surface. The heat transfer coefficient for a vertical surface of length L can be expressed in terms of the modified Nusselt number of different flow regimes of the condensate. In the laminar wave free region this is

$$\frac{\bar{h}_L \left(\frac{\mu_{lf}^2}{\rho_{lf}^2 \cdot g} \right)^{1/3}}{\lambda_{lf}} = 1.47 Re_{lf}^{-1/3} \quad Re_{lf} \leq 30 \quad (9)$$

g is the gravitational acceleration. In the laminar wavy region this becomes

$$\frac{\bar{h}_L \left(\frac{\mu_{lf}^2}{\rho_{lf}^2 \cdot g} \right)^{1/3}}{\lambda_{lf}} = \frac{Re_{lf}}{1.08 \cdot Re_{lf}^{1.22} - 5.2} \quad 30 \leq Re_{lf} \leq 1800 \quad (10)$$

and in the turbulent region

$$\frac{\bar{h}_L \left(\frac{\mu_f^2}{\rho_f^2 \cdot g} \right)^{1/3}}{\lambda_f} = \frac{Re_f}{8750 + 58 Pr_f^{-0.5} \cdot (Re_f^{0.75} - 253)} \quad Re_f \geq 1800 \quad (11)$$

Pr is the Prandtl number of the condensate film.

The heat transfer coefficient of the wall, h_{wall} , in Eq.3e can be easily obtained by dividing the thermal conductivity of the wall material by its thickness. In Eq.3f, h_{cool-w} depends on the flow conditions of the cooling water. This has to be calculated or can be obtained from correlations in literature.

Condensation is a complex phenomenon where conditions in the gas phase, the liquid film, the wall and the cooling water side determine its strength. Any change in any condition eventually effects condensation.

Due to the complexity commercial CFD packages do not include the ability to model surface condensation. Depending on the strength of condensation the gas flow changes completely, which increases the need for additional coding to CFD packages. As density of water is 3 orders of magnitude larger than that of vapour condensation has an effect on the volume flow. E.g. in case of a pure vapour flow where 50 % condenses the flow conditions would be calculated completely wrong as the volume flow of the gas would be 100% overestimated. Figure 3 and 4 show results of a calculation for a vapour / N₂ mixture in a vertical tube. This calculation was performed using a simplified condensation code where heat transfer resistances are not considered and the condensing temperature was kept constant. Despite the approximations the effect of the decreasing vapour mass on the velocity and temperature profiles can be seen clearly. The boundary conditions and dimensions used were the following

Dimensions	Diameter	0.022m	scaled 10:1
	Length total	1 m	scaled 1:1
	Entrance length	0.2m	no heat transfer
	Condensing length	0.8m	
Temperature	Inlet	473 K	
	Condensing wall	294 K	kept constant
Velocity	max. value	12.24 m/s	parabolic profile
Mass fractions	Vapour	0.75	
	N ₂	0.25	
Pressure		1 bar	
Turbulence model k-ε two-layer zonal model			

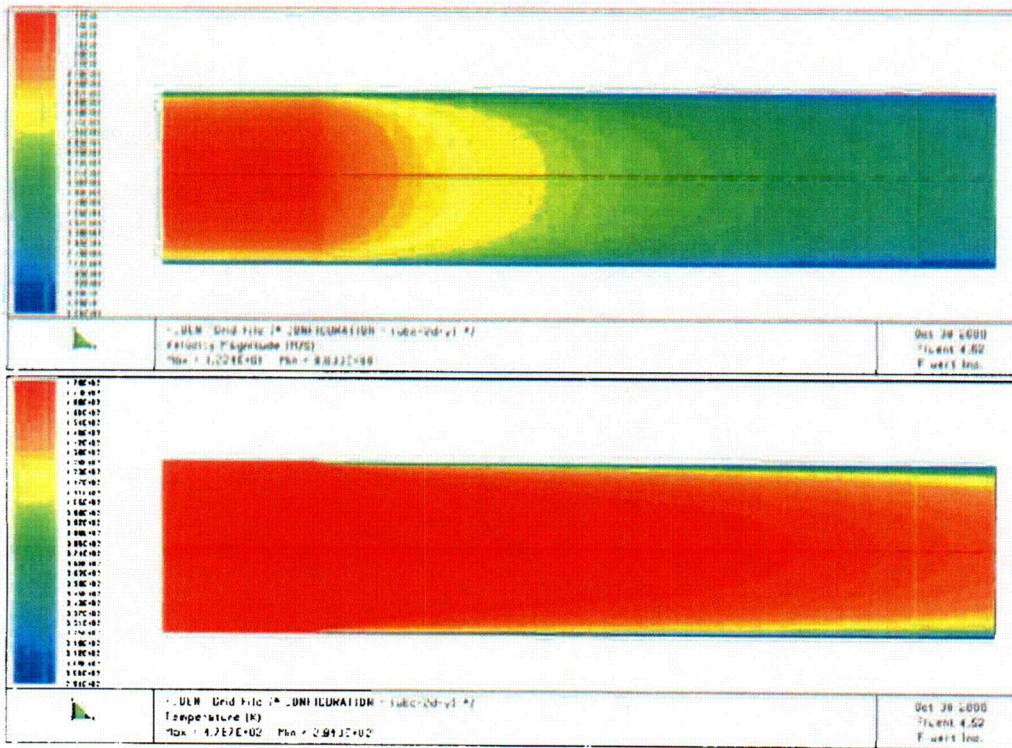


Fig. 3 Above: Velocity profile in condensing conditions ($v_{\max}=12.24$ m/s). Below: Temperature profile ($T_{\max}=473$ K, $T_{\min}=294$ K)

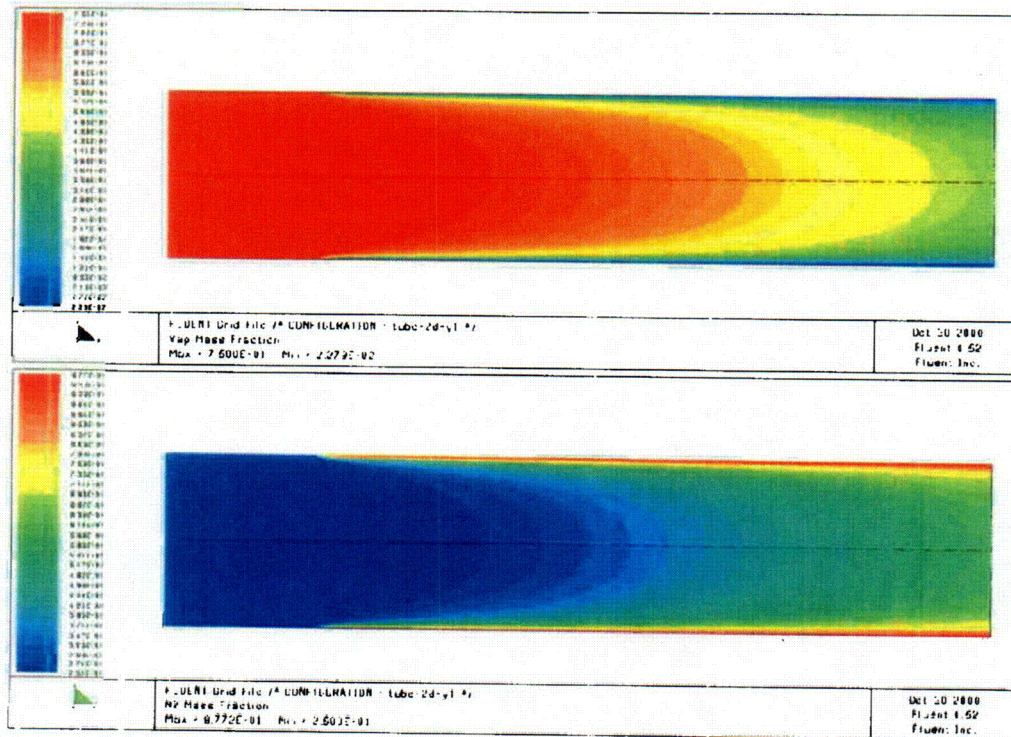


Fig. 4 Above: Mass fraction profile of vapour (max=0.75, min=0.02). Below: Mass fraction profile of N_2 (max=0.98, min=0.25).

As explained before the effect of the interface temperature is important. However, this importance depends on the temperature range and is little in the example shown above as the saturated vapour pressure (FIG.2) does not change significantly by changing the temperature e.g. 10 K (294 ± 10 K). This importance increases tremendously with increasing interface temperature. Thus, T_{inf} has to be calculated using Eq.(1b - 11). This is a two-phase flow problem a commercial CFD package like Fluent is not able to solve. Fluent offers two-phase modelling applications for a dispersed second phase (spray) or a free surface (wave modelling for ship design). Neither model is applicable for modelling condensation. Therefore the Aerosol Technology Group of VTT Energy is developing an additional code to account for the interface temperature. Fluent calculates the gas phase, with the temperature on the edge of the computational domain set equal to the interface temperature calculated in subroutines based on Eq.(1b - 11).